

1 **Estimating changes in temperature distributions in a large ensemble of**  
2 **climate simulations using quantile regression**

3 Matz A. Haugen\*, Michael L. Stein and Elisabeth J. Moyer

4 *University of Chicago, Chicago, USA*

5 Ryan L. Sriver

6 *University of Illinois at Urbana-Champaign, Urbana, USA*

7 \*Corresponding author address: Matz A. Haugen, 5734 S. Ellis Ave, 60637, Chicago, USA.

8 E-mail: mahaugen@uchicago.edu

## ABSTRACT

9     Understanding future changes in extreme temperature events in a transient  
10 climate is inherently challenging. A single model simulation is generally in-  
11 sufficient to empirically characterize the statistical properties of the underly-  
12 ing physical processes governing the climate. Ensembles of repeated simula-  
13 tions (with different initial conditions providing independence) greatly expand  
14 the amount of data available, which in turn allows new approaches for charac-  
15 terizing changes in extremes. We present here one such new approach, using  
16 ensembles that allow characterizing changes in temperature distributions us-  
17 ing a continuous representation of seasonality rather than breaking the dataset  
18 into seasonal blocks. That is, we assume that temperature distributions evolve  
19 smoothly both day-to-day over an annual cycle and year-to-year over longer  
20 secular trends. To demonstrate our method’s utility, we analyze an ensem-  
21 ble of 50 simulations of the Community Earth System Model (CESM) under  
22 a scenario of increasing radiative forcing to 2100, focusing on North Amer-  
23 ica. The results both confirm aspects of climate system behavior known from  
24 previous studies and also elucidate new features. Confirming results include  
25 that daily temperature bulk variability generally decreases in wintertime in the  
26 continental mid- and high-latitudes ( $> 40^\circ$ ). One new result is that these same  
27 wintertime distributions, the low tails “stick”, i.e. experience a lesser reduc-  
28 tion in variability, producing a more negative skew. Although the examples  
29 above concern temperature only, the technique is sufficiently general that it  
30 can be used to generate precise estimates of distribution changes in a broad  
31 range of climate variables by exploiting the power of ensembles.

## 32 1. Introduction

33 Climate time series have generally been assumed to be separable into two components: random-  
34 ness inherent in the underlying physical processes, which we call natural variability, and climatic  
35 trends, e.g. in the form of forced secular trends that follow from increasing concentrations of  
36 greenhouse gases or seasonal trends. Recently, the degree to which natural variability may itself  
37 be changing has received significant scientific interest (e.g. Trenberth 2011; Donat and Alexander  
38 2012; Deser et al. 2012a; Thompson et al. 2015; Kay et al. 2015). Potential changes in climate  
39 extremes, because of their heightened societal impacts, are of special concern (e.g. Davison and  
40 Smith 1990; Stott et al. 2004; Chavez-Demoulin and Davison 2005; Eastoe and Tawn 2009; Otto  
41 et al. 2012; Swain et al. 2014; Singh et al. 2014; Trenberth et al. 2015; Diffenbaugh et al. 2015;  
42 Huang et al. 2015a; Jalbert et al. 2017). However, fully characterizing this evolving natural vari-  
43 ability of rare events is intrinsically challenging due to the limited amount of available observations  
44 or simulation data. The long equilibration time of the climate system means that on the timescales  
45 of interest to human society, the climate state will be evolving, so that its statistical properties are  
46 not stationary. Studies of future climate extremes often employ statistical extreme value theory to  
47 make inferences about rare events with modest amounts of data (Swain et al. 2014).

48 In this work, we study the entire distribution of temperatures in a transient climate, including  
49 rare events, by employing quantile regression on an ensemble of simulations of an identical forcing  
50 scenario from a single climate model. Given sufficient care in choosing different initial conditions,  
51 such a large ensemble will reflect the natural variability of the system, since each simulation will be  
52 statistically independent in terms of its natural variability. The increased data provided by multiple  
53 simulations then admits more confident statements about changes in the statistical behavior of the  
54 system than can be made with a single simulation. While the use of ensembles is a relatively recent

55 development, it is growing rapidly (e.g. Deser et al. 2012b,a, 2014; Fischer and Knutti 2014; Kay  
56 et al. 2015; Sriviver et al. 2015; Rodgers et al. 2015; Hagos et al. 2016). Deser et al. (2012b),  
57 Deser et al. (2012a) and Fischer and Knutti (2014) in particular discuss how ensembles help in  
58 distinguishing internal climate variability from anthropogenic effects and allow more accurate  
59 estimates for the forced model response.

60 Ensembles of multiple simulations offer at least three advantages that are currently under-  
61 exploited. The most obvious advantage is that the increased data volume allows examining the  
62 entire distribution of a climate variable. Studies of climate variability to date are generally di-  
63 vided between those that address the center of the distribution (e.g. Semenov and Bengtsson 2002;  
64 Räisänen 2002; Kitoh and Mukano 2009; Screen 2014; Schneider et al. 2015), and those that  
65 address its tails (e.g. Katz and Brown 1992; Meehl et al. 2009; Northrop and Jonathan 2011;  
66 Davison et al. 2012; Huser and Davison 2014; Trenberth et al. 2015; Huang et al. 2015b; Jal-  
67 bert et al. 2017), generally via extreme value theory. A more limited body of studies address  
68 overall distributional changes in climate variables, but these generally focus on observations or  
69 observation-based data products, which are necessarily limited in terms of data amount and there-  
70 fore require spatial or temporal aggregation (Donat and Alexander 2012; Stainforth et al. 2013;  
71 Chapman et al. 2013; Huybers et al. 2014; McKinnon et al. 2016; Rhines et al. 2017). Aggregat-  
72 ing data spatio-temporally requires stationarity assumptions of the signal or explicitly modeling  
73 the spatio-temporal dependence. When studying model projections using ensembles, the large  
74 amount of data at each location allows us to accurately estimate changes in the distribution of  
75 climate variables (e.g. temperature) without spatial aggregation.

76 A second potential advantage provided by data-rich ensembles is that trends in both means  
77 and variability need not be modeled as linear in time (Franzke 2015; Gao and Franzke 2017).  
78 Typically, analyses assume linear trends, but in realistic scenarios, forcings are not linear over

centennial timescales, and a linear approximation can be misleading (see for example Poppick et al. 2017). The increased data provided by ensembles means that we can consider more flexible statistical models to better represent complex climate responses. As we will show, distributions of daily temperature evolve nonlinearly, and follow different trajectories even as a function of quantiles (i.e. different parts of the distribution). Analysis methods should therefore be able to take into account nonlinearities both in time and across quantiles.

Finally, a third advantage of ensembles is that they allow a more natural treatment of seasonal variation in climate variables. In situations of limited data, it is standard practice to treat seasons separately, assuming that each season has a temporally constant average and stationary statistical properties discontinuous from neighboring seasons. With ensembles of simulations, we can allow for a smooth change in the underlying trend from day to day, using a parsimonious set of parameters. By modeling the entire year on a continuum, we can explore how each season transitions to the next and how seasonal patterns change over time, features that may be highly dependent on both geographic location and quantile.

We describe here a methodology for exploiting ensembles to study changing climate variability that captures these advantages: we model the complete distribution of daily temperatures as a continuous function of both seasonality and secular climate change over time. Although the methodology is applied to temperature here, it is general and can be applied to other climate variables of interest. We also show how such an ensemble-based approach is well-positioned for the purposes of uncertainty quantification. Because each simulation is treated as an independent sample drawn from the ensemble of simulations, we circumvent the issue of dependency within each simulation. We can therefore obtain uncertainty quantifications for all estimates by resampling complete simulations from the ensemble.

102 In the sections that follow, we describe estimated changes in both bulk and tail variability as  
103 differences in two quantiles; a large quantile difference implies more variability in a given region  
104 of the distribution. When those quantiles lie in the high or low tails, the quantile difference is a  
105 measure of the spread or thickness of the tail. Figure 1 gives a pictorial explanation of how quantile  
106 differences reflect bulk and tail variability. Although the estimated model is seasonally continuous,  
107 we also present results assuming seasonally constant conditions, and show that the seasonal effect  
108 on temperature can indeed be explained with a reasonably smooth function. When applied to  
109 model runs of a realistic future climate scenario, results reproduce some well-understood changes  
110 (e.g. strong reduction in wintertime variability at continental mid-latitudes) and produce some new  
111 insights (e.g. strong changes in skewness driven by low tail behavior).

## 112 2. Data

113 We apply our algorithm to an ensemble of 50 historical/future simulations of the Community  
114 Earth System Model (CESM) (Sriver et al. 2015). The atmospheric component is the low-  
115 resolution Community Atmosphere Model version 4, with T31 spectral resolution ( $\sim 3.75^\circ \times$   
116  $3.75^\circ$ ) and 26 vertical levels. The model ocean component is the low-resolution version of the  
117 Parallel Ocean Program version 2 (Smith et al. 2010) with a nominal horizontal grid resolution of  
118  $3^\circ$ , augmented to approximately  $1^\circ$  at the equator. The ocean model contains 60 vertical levels,  
119 down to a maximum depth of 5,500 m.

120 The ensemble is especially appropriate for the purpose of studying variability because it is based  
121 on a  $\sim 10,000$  year pre-industrial control simulation. After a  $\sim 4000$  year spin-up using constant  
122 preindustrial conditions, 50 historical hindcasts (1850-2005) are initialized from snapshots of the  
123 coupled model state taken every 100 years, so that the last hindcast is initialized after approxi-  
124 mately 9000 years of the control simulation. Each hindcast is then extended to 2100 using the

125 Representative Concentration Pathway (RCP) 8.5 scenario. The 100-year gap between each new  
126 initialization ensures nearly independent ensemble members that fully capture internal variability  
127 within the coupled system. RCP8.5 corresponds to anthropogenic radiative forcing of roughly 8.5  
128  $\text{W m}^{-2}$  by 2100 (Moss et al. 2010). More information about the model and ensemble design can  
129 be found in Sriver et al. (2015).

130 CESM does show some known biases that affect primarily temperature means (and possibly  
131 trends in means), but also to some extent the higher-order moments of the temperature distribution,  
132 e.g. variance and skewness. Known model biases include reduced ocean heat transport, low north  
133 Atlantic sea surface temperature, and excessive northern hemisphere sea ice (Shields et al. 2012).  
134 The model generally underestimates both temperature and precipitation extremes compared with  
135 observations, i.e. the mean of the extreme value distributions is biased, but the scale and shape are  
136 consistent with observations for the continental United States (Sriver et al. 2015).

137 To evaluate whether the CESM simulations provide sufficiently realistic temperature distribu-  
138 tions for the purpose of this analysis, we compare CESM temperatures with those from the ERA-  
139 Interim (European Reanalysis) data product (Dee et al. 2011). Figure 2 shows the model/reanalysis  
140 comparison for winter; for summer see Supplementary Online Material Figure S1. The model un-  
141 derestimates variability in some places, and produces excessively cold winter temperatures in the  
142 Arctic. The resulting exaggerated temperature gradients contribute to excess variability and ex-  
143 cessively negative skew in the northern mid-latitudes. Skewness is proportional to the cube of  
144 temperature after subtracting off the average seasonal temperature; see Appendix A1. Throughout  
145 this work, we will show in-depth analysis from three locations with distinct temperature distri-  
146 butions to highlight our proposed method (**a**, **b**, and **c** shown in Figure 2). See Supplementary  
147 Online Material Figure S2 for comparison of model and reanalysis temperature distributions in  
148 both summer and winter for these locations.



### 3. Methods

In the methodology presented here, we model temperature at each location as a function of both seasonality and long-term change of the annual temperature distribution. We use two independent variables, with seasonality represented by a variable  $d$ , the day of the year (spanning values 1 to 365), and change in annual temperature represented by a variable  $t$ , years elapsed since 1850 (spanning 0 to 250 for these scenarios). We thus assume that each temperature quantile can be described by two sets of basis functions that represent the two variables' independent relationships with temperature (called here  $\{f_i(d)\}$  and  $\{g_j(t)\}$ ), and interaction terms  $h_i(d)s_j(t)$ , where  $f_i, g_j, h_i$ , and  $s_j$  are all smooth functions of the appropriate variable. The interaction terms are required to capture effects in which long-term temperature evolution differs between seasons, e.g. the robust projection that winter temperatures warm more than summer temperatures. To impose our smoothness condition, we assume that  $f_i, g_j, h_i$ , and  $s_j$  are piecewise cubic polynomials with a continuous second derivative, also called splines. (For a review of cubic polynomial basis functions, see Hastie et al. 2009, Chapter 5.) Because the seasonality variable  $d$  is periodic, its basis functions are also assumed periodic. For more details, see Appendix A2a.

We choose the number of basis functions by evaluating a metric representing model adequacy. Our model sufficiency criterion is aimed at capturing the long term underlying signal. We do not require estimated quantile functions to capture transient events during the historical period like volcanic eruptions. Details on how we select the number of basis functions is given in Appendix A2b. In our climate simulation output, the intra-seasonal effect requires more detailed modeling than the inter-seasonal effect. In the results shown here, we fit the model with 15 terms (that is, basis functions) for the main seasonal effect  $\{f_i\}$ , but the interaction terms require less seasonal complexity, so we use only 3 terms for  $\{h_i\}$ . We use 4 terms for both the temporal change  $\{g_j\}$

172 and the interaction terms  $\{s_j\}$ . That is, modeling long-term change generally requires fewer terms  
 173 than modeling seasonality. In summary, we use 32 basis functions in total including an intercept  
 174 term. We then fit each  $q$  quantile of temperature

$$T_q(d, t) = \alpha + \sum_i a_i f_i(d) + \sum_j b_j g_j(t) + \sum_{i,j} c_{i,j} h_i(d) s_j(t), \quad (1)$$

175 where all of the coefficients depend on  $q$  but we suppress the dependence for convenience. This  
 176 fit determines coefficients  $a_i, b_j, c_{i,j}$  for each quantile at each location.

177 To simplify notation, we construct a matrix  $X$  where each column contains a basis function and  
 178 each row refers to a unique value of  $d$  and  $t$ . Using this matrix,  $X$ , we construct our temperature  
 179 model in vectorized form,

$$T_q = X\beta_q, \quad (2)$$

180 where  $\beta_q$  contains the basis coefficients  $a_i, b_j, c_{i,j}$ . The predictor matrix  $X$  will have 32 columns,  
 181 each corresponding to one basis function, and  $365 \times 250 \times 50$  rows, where each row is a daily  
 182 average temperature. Similarly,  $\beta_q$  will be a 32-length vector. To get a confidence interval around  
 183  $T_q$ , we re-estimate the coefficients,  $\beta_q$ , using a resampled data set. Because we have 50 simulations  
 184 we resample the data by drawing whole simulations from our ensemble of 50 simulations. By  
 185 resampling complete realizations, the dependency structure within realizations is maintained in  
 186 the resampled data. Thus, repeating this resampling and re-estimation procedure 100 times yields  
 187 pointwise confidence bands around each estimated  $T_q$ . Appendix A2c provides further details  
 188 about uncertainty quantification.

189 As an example of a typical model fit, we show in Figure 3 the seasonal cycle in CESM daily  
 190 temperatures for three locations, along with estimates of low, median and high quantiles. We show  
 191 here data from 1850 to demonstrate the seasonal fit rather than that of the long-term trend. All  
 192 locations show strong seasonal differences in variance that are well-represented by our smooth

estimates. Relevant features that are captured include an asymmetrical seasonal cycle in all locations; a clear left skewness in wintertime in all three locations (although most pronounced in the higher-latitude **a** and **b**); and a distinct springtime shoulder in the higher-latitude locations. These characteristics show the benefit of explicitly modeling seasonal variations as smoothly varying functions as opposed to a set of four constant functions changing value with season. Nuances like the decrease in winter temperature spread (variability) from early to late winter would not be captured by a piecewise constant model.

## 4. Results

To facilitate comparison to previous studies, we first perform a preliminary analysis where we replicate more standard methods. That is, we examine changes in the aggregate distribution of temperatures over multi-week and multi-month intervals, before we show results from our new approach that calculates responses for individual days. Even the standard analysis readily shows that temperature distributions in the CESM ensemble change over the RCP 8.5 scenario (Figures 4, 5, and 6, which compare the initial and final time windows 1850-1864 and 2086-2100). Means uniformly shift warmer, but the shapes of the distributions also change in terms of variance and skewness. Figure 4 shows initial and final distributions in our example locations for aggregated 15-day periods in winter and summer. In at least two of the three depicted locations, it is clear that the distributions are becoming narrower, although quantifying exactly how the tails are changing requires a quantification of the tail size and shape.

Regarding the spatial characteristics of temperature distributions, we see the expected strong decrease in variance in winter over land, especially in the northern mid-latitudes (Figures 5 and 6). By contrast, summer variance changes are much smaller and differ in sign in different locations. Temperature skewness, i.e. the asymmetry of the distribution, shows strong changes in winter

216 over land in a dipole pattern. Winter temperature distributions are in all time periods negatively  
217 skewed throughout most of the domain, but in the north (including locations **a** and **b**), they become  
218 more negatively skewed in the future, while in the south (including location **c**), they become more  
219 symmetric. Summer skewness changes are again smaller and with less spatial coherence, other  
220 than the strong transitions in the Southern Great Plains and in Mexico/Central America, where  
221 skewness in temperature distributions actually changes sign.

222 With a smooth estimate of quantiles of average temperature, we show that the onset of spring, as  
223 measured by the first day of the year where the .5 quantile estimate reaches  $-2.2^{\circ}\text{C}$  (Pearse et al.  
224 2017), occurs earlier in the year as the climate warms in the Detroit area (see Figure 7). The lower  
225 quantiles seem to be progressing faster than the .5 quantile, with the .25 quantile hitting the  $-2.2^{\circ}\text{C}$   
226 mark at a rate of approximately 15 days earlier per decade at present times. Note also that the .5  
227 quantile never goes below the threshold after year 2080. It is unclear how to produce the equivalent  
228 results using existing methods of segmenting average temperature into seasons. For instance, if we  
229 were to look at quantiles of average temperature during winter the edges of the season would pull  
230 the overall quantile estimates up and prematurely estimate the onset of spring. Moreover getting  
231 information regarding the average temperature of a specific day would be impossible with seasonal  
232 averaging.

233 Our methodology for quantile estimation provides additional information that helps to quantify  
234 how temperature distributions are changing and to estimate the uncertainty associated with each  
235 change. We can evaluate not only bulk variability – the interquartile range (IQR), the difference  
236 between the 0.25 and 0.75 quantiles – but differences between any two quantiles. We therefore  
237 evaluate the difference between two low or high quantiles, denoted  $\Delta q_{low}$  and  $\Delta q_{high}$ , which mea-  
238 sure tail variability in the same way that interquartile range measures the variability of the bulk  
239 distribution. If the skewness of a distribution changes over time, then future distributions are not

240 simply scaled versions of present distributions. That is, their tail variabilities must change differ-  
 241 ently than does the IQR. In the case of the northern mid-latitudes winter temperatures shown in  
 242 Figure 5, where distributions become more negatively skewed as bulk variability decreases in the  
 243 future, the effect could result from either/both a low tail contracting less than the bulk (or actu-  
 244 ally increasing), or a high tail contracting more than the bulk. Our methodology allows readily  
 245 differentiating these cases.

246 To assess whether the high tail and/or the low tail is driving changes in skewness, we consider  
 247 the fractional changes in low, high, and bulk variability. If we denote the initial and final quantile  
 248 difference as  $\Delta q_{q,i}$  and  $\Delta q_{q,f}$  at the  $q$  quantile, the temporal change in quantile differences relative  
 249 to the initial year is then

$$\rho = \frac{\Delta q_{q,f} - \Delta q_{q,i}}{\Delta q_{q,i}}. \quad (3)$$

250 Because we model the complete temperature distribution for each day of the year for all years,  
 251 we choose a representative day to understand winter and summer changes (Jan 1 and July 5,  
 252 respectively), and consider the difference between the beginning and end of the scenarios, the  
 253 years 1850 and 2000. For these representative days, we show in Figure 8 the fractional variability  
 254 changes of  $\rho$  for low and high tails as well as the IQR.

255 Results show that tail changes can indeed differ strongly from changes in the bulk of the distribu-  
 256 tion. In wintertime (Figure 8, top row), in much of the northern mid-latitudes (including locations  
 257 **a** and **b**), low tails change in a way that contributes to a more negative skew. Low tail variability  
 258 contracts less than does the IQR, while high tail variability contracts more strongly. (High tails  
 259 would contribute to more negative winter skew predominantly in the Hudson Bay region, where  
 260 the model shows distinct bias.) In summertime (Figure 8, bottom row), the high tail dominates the  
 261 transition to positive skew in the Southern Great Plains region (including location **c**).

262 To clarify the relative contributions of high and low tails to skewness changes, we also examine  
263 evolving temperature variability in the bulk and tails as a function of seasonality as well as long  
264 term change. Figure 9 shows absolute variability changes for the three example locations **a**, **b**,  
265 and **c** estimated using our quantile model, and for fractional changes see Supplementary Online  
266 Material Figure S6. The uncertainty around our estimates is quantified by resampling the original  
267 simulations (with replacement) and recomputing the estimates using this new set of simulations  
268 (see Appendix A2c for details). In all locations, wintertime skewness changes are driven by the  
269 relative changes in IQR and low tails. In the higher-latitude locations **a** and **b**, more negative winter  
270 skew results because the IQR contracts even more strongly than does the low tail variability. In  
271 other words, the low tails “stick”. In the lower-latitude location **c**, more positive winter skew  
272 results because the IQR barely changes while the low tail variability contracts strongly.

273 The complexity of the relationships in Figure 9 also shows how misleading it may be to use a  
274 three-month block to represent a season. While all three locations show larger IQR in winter than  
275 summer, the transition from winter to summer happens more quickly in some locations than at  
276 others, more abruptly in the northernmost location **a** and more gradually in **c**. Low-tail variability  
277 seasonal transitions are even sharper than those of IQR in **a** and **b**, but more gradual in **c**. In  
278 contrast, high-tail variability is more seasonally constant overall than low-tail variability. Through  
279 these examples, we see how our method offers detailed information about changes in variability  
280 across seasons and annual change, usually unavailable when analyzing each season separately.

281 While we show only three locations in the text here, an online interactive application allows  
282 similar in-depth examination of changes in model temperature distributions at all locations within  
283 North America, available at <https://matzhaugen.com/links.html>. The application allows the user to  
284 browse through any desired location to see how the variability changes as a function of season,

year and quantile difference. We include temperature histograms of the first and last simulation year for the designated location, as well as maps that show the variability change spatially.

## 5. Conclusions

We present a method to quantify changes in tail variability of temperature with high precision in a transient climate model. Using data from the whole year and the whole span from 1850-2100 we estimate temperature quantiles as a function of seasonality and long term change. Analyzing the whole year simultaneously as opposed to analyzing each season separately allows for more flexible modeling of seasonality. The large ensemble makes it possible to fit such models stably.

By resampling entire simulations from the ensemble of climate simulations and recalculating the quantiles, we obtain confidence bands that do not require any assumptions of independence within any one simulation. We show that the smooth quantile estimates are accurate even across small intervals of the domain of the predictors. The fidelity of these intervals serves as a criterion to determine the required complexity in the statistical model.

The techniques presented in this study are validated in part by the fact that they replicate several prior conclusions made in the literature, e.g. the well-known projected decrease in winter variability in the northern mid-latitudes (e.g. Schneider et al. 2015) most likely due to amplified warming in the arctic (Screen 2014). Our approach furthermore allows us to quantify tail variability and give corresponding confidence intervals around our estimates. In the case study of CESM runs analyzed here, we relate the changes in tail variability to changes in skewness of the temperature distributions, and find that in most of the domain analyzed, wintertime skewness changes are driven largely by the relative behavior of IQR and low tails. For example, in much of the continental northern U.S. and Canada, the low tail of temperature contracts substantially less than does the overall temperature variability.

308 These results may inform physical explanations for the projection that skewness in winter tem-  
309 perature changes in a dipole pattern across North America. It is possible that the skewness change  
310 is a result of a change in the mean location and variability of the mid-latitude jet stream (e.g.  
311 Barnes and Polvani 2013); this possibility may warrant further study.

312 The abundance of data available in ensemble simulations relative to single simulations allows  
313 using quantile regression to accurately estimate high quantiles, avoiding some of the limitations  
314 of extreme value theory. Unlike quantile regression, methods using extreme value theory require  
315 making assumptions about the shape of the tail of the distribution. By parameterizing the season-  
316 ally time-varying distribution of temperature through smooth functions using the whole year as  
317 our domain, we also reveal previously unavailable details about seasonal transitions. For example,  
318 we show here that springtime variability decreases occur later in the year at lower latitudes, and  
319 that seasonal transitions in tail variability differ from those in IQR. While we analyze only tem-  
320 perature here, our method is intended to be general enough to be applied to other climate variables  
321 such as precipitation or humidity. These detailed insights into climate variable distributions may  
322 be valuable for risk assessment studies that emphasize extreme events.

## 323 **Acknowledgments**

324 This work was supported in part by STATMOS, the Research Network for Statistical Methods  
325 for Atmospheric and Oceanic Sciences (NSF-DMS awards 1106862, 1106974 and 1107046), and  
326 RDCEP, the University of Chicago Center for Robust Decision-making in Climate and Energy Pol-  
327 icy (NSF grant SES-0951576). We acknowledge the University of Chicago Research Computing  
328 Center, whose resources were used in the completion of this work. Ryan L. Sriver acknowledges  
329 support from the Department of Energy sponsored Program on Integrated Assessment Model De-



330 velopment, Diagnostics and Inter-Model Comparisons (PIAMDDI), and the Program on Coupled  
331 Human Earth Systems (PCHES).

## A1. Model and reanalysis comparisons

Following the discussion on the paper, we define sample mean, variance and skewness as

$$\begin{aligned}\bar{x} &= \frac{1}{n} \sum_{i=1}^n x_i \\ s^2 &= \frac{1}{n} \sum_{i=1}^n (x_i - \bar{x})^2 \\ \gamma &= \frac{1}{n} \sum \left( \frac{x_i - \bar{x}}{s} \right)^3.\end{aligned}\tag{A1}$$

These definitions are used in Figures 2, 5, and 6 in the main text and in Supplementary Online Material Figures S1 and S2. We plot the standard deviation  $s$  rather than the variance  $s^2$ .

## A2. Model Details

In the following, we first give details regarding the regression of temperature quantiles on a fixed set of basis functions. We then discuss how to select the number of basis functions, through a “sufficiency criterion”. Lastly, we describe how we quantify uncertainty in the quantile estimates.

### a. Model estimation

Given the number of basis functions in our model, represented by the columns in a matrix  $X$  with number of rows equal to the number of observations in the data set, we construct our temperature quantile estimate,  $\hat{T}_q$ , and corresponding coefficients,  $\hat{\beta}_q$ , viz.

$$\hat{T}_q = X\hat{\beta}_q\tag{A2}$$

such that the  $q^{th}$  fraction of residuals between the observations  $T$  at a particular location and their estimates,  $T - \hat{T}_q$ , are greater than zero and a fraction  $1 - q$  are less than zero. With the

temperature model in Equation 2, our coefficient vector estimate,  $\hat{\beta}$ , contains the estimates of  $a_i, b_j, c_{i,j}$ . Note that the seasonal interaction terms corresponding to the coefficients  $c_{i,j}$  are not necessarily the same as the main seasonal terms corresponding to  $a_i$ . In fact, we find that fewer seasonal interaction terms are needed to describe the interaction behavior.

Computationally, obtaining the above quantile is equivalent to solving the following optimization problem (Koenker and Bassett Jr 1978),

$$\min_{\beta} \left\{ \sum_{d,t: T(d,t) \geq X(d,t)\beta} q|T(d,t) - X^T(d,t)\beta| + \sum_{d,t: T(d,t) < X(d,t)\beta} (1-q)|T(d,t) - X^T(d,t)\beta| \right\}, \quad (\text{A3})$$

and can be implemented in either R or MATLAB using existing libraries<sup>1</sup>. Because we have access to 50 simulations, each location provides us with  $365 \times 250 \times 50$  or approximately 4.5 million observations. Consequently, even fairly high quantiles can be accurately estimated without borrowing data from neighboring locations through a spatial model as done by e.g. Reich et al. (2011). However, making inferences about more extreme quantiles, such as the quantiles .001 or .999, cannot be guaranteed to work as well with our methods.

We do not experience issues with quantile estimates crossing in our study area even though the optimization framework above does not explicitly enforce monotonicity with increasing quantile estimates. The absence of crossing quantiles is likely also due to the large sample size. For strict enforcement of monotonicity in the quantile curves see e.g. Bondell et al. (2010).

---

<sup>1</sup>We use the R library `rq` and the function `rq.fit.pfn`, developed by Portnoy and Koenker (1997). Basis functions are created using `pbs` for periodic spline basis functions and `ns` for non-periodic splines. The non-periodic splines are constrained to be linear beyond the domain, 1850-2100, and are called *natural splines*.

### 363 *b. Model selection*

364 We describe our approach to selecting a modest set of basis functions that can accurately rep-  
 365 resent the temperature data. If the model chosen has too many basis functions we run the risk of  
 366 overfitting out-of-sample observations. To make sure this does not happen we need a metric to  
 367 quantify the goodness-of-fit of the model.

368 Any reasonable temperature model we fit to the data will by definition contain the desired  
 369 amount of positive and negative residuals *globally* according to the desired quantile  $q$ . A more  
 370 stringent requirement would be that the smooth temperature estimate contains approximately an  
 371 appropriate fraction of positive and negative residuals on a *daily* basis: for each  $d$  and  $t$ ,

$$S(d, t) = \frac{1}{n} \sum_{i=1}^n I [\hat{T}_i(d, t) - T_i(d, t) > 0] \approx q, \quad (\text{A4})$$

372 where  $I$  is the indicator function and  $n$  is the total number of samples (i.e. 50 for our CESM  
 373 ensemble data set). If  $S(d, t)$  is close to the value  $q$  for each  $d$  and  $t$ , the model would accurately  
 374 describe the data and the number of basis functions is sufficient. In reality, we are looking basis  
 375 functions that obey A4 with  $d$  averaged over blocks of days to increase the sample size, e.g. 10  
 376 days blocks. It is also not the goal to capture the quantile at too short a timescale as events like  
 377 volcanic eruptions would interfere with the estimate.

378 In order to estimate the appropriate number of basis functions, we hold out 5 simulations from  
 379 the fitting process and use these to calculate our exceedences, which we call  $S_{test}(d, t)$ . We repeat  
 380 this 10 times so that all the simulations are eventually held out, giving 10 samples of  $S_{test}(d, t)$ . As  
 381 we increase model complexity through degrees of freedom in the basis functions, the variability  
 382 of  $S_{test}$  should reach a minimum when the necessary number of basis functions is reached and  
 383 the quantile estimate is the same for each time point. If the number of basis functions is increased  
 384 beyond this point, we start to overfit the data and the out-of-sample variability of  $S_{test}$  will increase.

385 To estimate  $S_{test}$ , we block the variables in two ways, one for each variable. First, we divide  
 386 each year in 10-day bins and calculate the average exceedence estimate,  $\hat{S}_{test}$ , in each bin. We  
 387 sum over the whole domain of long term change,  $t$ , and a subset of the seasonality variable,  $d$ .  
 388 Specifically, let  $A$  be a set of non-overlapping contiguous blocks of days that together cover the  
 389 whole year, where  $a_j$ ,  $j = 1, \dots, m$  are the elements of the set. Also let  $T$  be the index set for  
 390 long term change,  $T = [1850, 2100]$ , measured in years. Then, for all  $a_j \in A$ ,

$$\hat{S}_{test}(a_j) = \frac{1}{n} \sum_{i=[1,n], d \in a_j, t \in T} I[\hat{T}_i(d, t) - T_i(d, t) > 0]. \quad (A5)$$

391 To get an equal number of days in each bin we use the first 360 days of the year only.

392 Second, we divide the long term change variable,  $t$ , in bins and repeat the process by flipping the  
 393 role of the variables in Equation A5 to get a set of  $\hat{S}_{test}(b_j)$  with  $b_j \in B$ , a set of non-overlapping  
 394 contiguous blocks of long-term change indices in  $T$ . An example of the blocked exceedence  
 395 estimate is shown in Figure 10. Note that the pointwise quantile estimate is contained between  
 396 the error bars, suggesting that the model is sufficiently complex. The standard deviation of these  
 397 estimates of  $\hat{S}_{test}$  is our measure of exceedence variability.

398 We seek the simplest model that gives good calibration of the quantile estimates (so close to 0.05  
 399 in Figure 10). At the same time we have to watch out to not overfit the data so we also want to  
 400 minimize out-of-sample variability. We find that a model with 15 seasonal, 3 seasonal-interaction  
 401 and 4 temporal degrees of freedom minimizes the variability of exceedences  $\hat{S}_{test}$ , shown in Figure  
 402 11, where seasonality has been binned. The out-of-sample fit when binning long-term change is  
 403 shown in Figure S7 in the supplement. Here, models 4-6 have approximately equal test error, so  
 404 since binning seasonality suggests the complexity of model 6, we chose model 6 as the overall  
 405 model. Including the possible interaction terms, the full model has 32 free parameters to be fitted,

406 or  $\hat{\beta} \in \mathbb{R}^{32}$ . All model candidates are shown in Table 1. We reach the same conclusion when  
407 blocking the long term change,  $t$ , and when analyzing different spatial locations (see Figure S7).

### 408 *c. Uncertainty Estimation*

409 With a reasonable model chosen through cross-validation, we present a way to quantify its uncer-  
410 tainty. Because we are using multiple simulations that are assumed independent, we resample en-  
411 tire simulations from the set of 50 simulations. Resampling 50 new simulations with replacement  
412 from the original set of simulations yields a new dataset. From the new data set we obtain another  
413 temperature estimate with the same model basis functions but different coefficients,  $\beta^*$ . After re-  
414 peating this resampling and re-estimating procedure 100 times we generate pointwise confidence  
415 intervals for temperature quantiles. For example, in Figure 9 we show the 90% confidence interval  
416 by selecting the pointwise .05 and .95 quantiles of temperature variability estimates. Because the  
417 confidence intervals are quite tight we deem the 100 new estimates (or bootstraps) sufficient to  
418 indicate that the results we describe in section 4 are not due to random variation. Larger number  
419 of bootstrap replicates might give slightly more accurate intervals but would not change our con-  
420 clusions. One might also consider fewer simulations as a compromise between computation time  
421 and quality of the estimates. Assuming normally distributed confidence intervals, we would expect  
422 the standard error to scale as  $1/\sqrt{n}$ . Thus, if one is willing to widen the confidence intervals by  
423 a factor of 2 (approximately) only 10 simulations would suffice. However, one could compensate  
424 for this greater variability by using fewer basis functions at a cost, of course, of obtaining less  
425 resolved estimates of seasonal patterns and long-term trends in the quantiles.

## References

- Barnes, E. A., and L. Polvani, 2013: Response of the midlatitude jets, and of their variability, to increased greenhouse gases in the CMIP5 models. *Journal of Climate*, **26** (18), 7117–7135.
- Bondell, H. D., B. J. Reich, and H. Wang, 2010: Noncrossing quantile regression curve estimation. *Biometrika*, **97** (4), 825–838.
- Chapman, S. C., D. A. Stainforth, and N. W. Watkins, 2013: On estimating local long-term climate trends. *Phil. Trans. R. Soc. A*, **371** (1991), 20120287.
- Chavez-Demoulin, V., and A. C. Davison, 2005: Generalized additive modelling of sample extremes. *Journal of the Royal Statistical Society: Series C (Applied Statistics)*, **54** (1), 207–222.
- Davison, A. C., S. A. Padoan, and M. Ribatet, 2012: Statistical modeling of spatial extremes. *Statistical science*, 161–186.
- Davison, A. C., and R. L. Smith, 1990: Models for exceedances over high thresholds. *Journal of the Royal Statistical Society. Series B (Methodological)*, 393–442.
- Dee, D. P., and Coauthors, 2011: The ERA-interim reanalysis: Configuration and performance of the data assimilation system. *Quarterly Journal of the royal meteorological society*, **137** (656), 553–597.
- Deser, C., R. Knutti, S. Solomon, and A. S. Phillips, 2012a: Communication of the role of natural variability in future North American climate. *Nature Climate Change*, **2** (11), 775–779.
- Deser, C., A. Phillips, V. Bourdette, and H. Teng, 2012b: Uncertainty in climate change projections: the role of internal variability. *Climate Dynamics*, **38** (3-4), 527–546.

Deser, C., A. S. Phillips, M. A. Alexander, and B. V. Smoliak, 2014: Projecting North American climate over the next 50 years: Uncertainty due to internal variability. *Journal of Climate*, **27** (6), 2271–2296.

Diffenbaugh, N. S., D. L. Swain, and D. Touma, 2015: Anthropogenic warming has increased drought risk in California. *Proceedings of the National Academy of Sciences*, **112** (13), 3931–3936.

Donat, M. G., and L. V. Alexander, 2012: The shifting probability distribution of global daytime and night-time temperatures. *Geophysical Research Letters*, **39** (14).

Eastoe, E. F., and J. A. Tawn, 2009: Modelling non-stationary extremes with application to surface level ozone. *Journal of the Royal Statistical Society: Series C (Applied Statistics)*, **58** (1), 25–45.

Fischer, E. M., and R. Knutti, 2014: Detection of spatially aggregated changes in temperature and precipitation extremes. *Geophysical Research Letters*, **41** (2), 547–554.

Franzke, C. L., 2015: Local trend disparities of european minimum and maximum temperature extremes. *Geophysical Research Letters*, **42** (15), 6479–6484.

Gao, M., and C. L. Franzke, 2017: Quantile regression–based spatiotemporal analysis of extreme temperature change in china. *Journal of Climate*, **30** (24), 9897–9914.

Hagos, S. M., L. R. Leung, J.-H. Yoon, J. Lu, and Y. Gao, 2016: A projection of changes in landfalling atmospheric river frequency and extreme precipitation over western North America from the Large Ensemble CESM simulations. *Geophysical Research Letters*.

Hastie, T., R. Tibshirani, and J. Friedman, 2009: *Elements of Statistical Learning*. 2nd ed., Springer.



- 467 Huang, W. K., M. L. Stein, D. J. McInerney, S. Sun, and E. J. Moyer, 2015a: Changes in US tem-  
 468 perature extremes under increased CO2 in millennial-scale climate simulations. *arXiv preprint*  
 469 *arXiv:1512.08775*.
- 470 Huang, W. K., M. L. Stein, D. J. McInerney, S. Sun, and E. J. Moyer, 2015b: Estimating changes  
 471 in temperature extremes from millennial scale climate simulations using generalized extreme  
 472 value (GEV) distributions. *arXiv preprint arXiv:1512.08775*.
- 473 Huser, R., and A. Davison, 2014: Space–time modelling of extreme events. *Journal of the Royal*  
 474 *Statistical Society: Series B (Statistical Methodology)*, **76** (2), 439–461.
- 475 Huybers, P., K. A. McKinnon, A. Rhines, and M. Tingley, 2014: US daily temperatures: The  
 476 meaning of extremes in the context of nonnormality. *Journal of Climate*, **27** (19), 7368–7384.
- 477 Jalbert, J., A.-C. Favre, C. Bélisle, and J.-F. Angers, 2017: A spatiotemporal model for extreme  
 478 precipitation simulated by a climate model, with an application to assessing changes in return  
 479 levels over North America. *Journal of the Royal Statistical Society: Series C (Applied Statistics)*.
- 480 Katz, R. W., and B. G. Brown, 1992: Extreme events in a changing climate: variability is more  
 481 important than averages. *Climatic change*, **21** (3), 289–302.
- 482 Kay, J. E., and Coauthors, 2015: The Community Earth System Model (CESM) large ensemble  
 483 project: A community resource for studying climate change in the presence of internal climate  
 484 variability. *Bulletin of the American Meteorological Society*, **96** (8), 1333–1349.
- 485 Kitoh, A., and T. Mukano, 2009: Changes in daily and monthly surface air temperature variability  
 486 by multi-model global warming experiments. *Journal of the Meteorological Society of Japan.*  
 487 *Ser. II*, **87** (3), 513–524.

- 488 Koenker, R., and G. Bassett Jr, 1978: Regression quantiles. *Econometrica: journal of the Econo-*  
489 *metric Society*, 33–50.
- 490 McKinnon, K. A., A. Rhines, M. P. Tingley, and P. Huybers, 2016: The changing shape of northern  
491 hemisphere summer temperature distributions. *Journal of Geophysical Research: Atmospheres*,  
492 **121 (15)**, 8849–8868.
- 493 Meehl, G. A., C. Tebaldi, G. Walton, D. Easterling, and L. McDaniel, 2009: Relative increase of  
494 record high maximum temperatures compared to record low minimum temperatures in the US.  
495 *Geophysical Research Letters*, **36 (23)**.
- 496 Moss, R. H., and Coauthors, 2010: The next generation of scenarios for climate change research  
497 and assessment. *Nature*, **463 (7282)**, 747–756.
- 498 Northrop, P. J., and P. Jonathan, 2011: Threshold modelling of spatially dependent non-stationary  
499 extremes with application to hurricane-induced wave heights. *Environmetrics*, **22 (7)**, 799–809.
- 500 Otto, F. E. L., N. Massey, G. J. Oldenborgh, R. G. Jones, and M. R. Allen, 2012: Reconciling two  
501 approaches to attribution of the 2010 Russian heat wave. *Geophysical Research Letters*, **39 (4)**.
- 502 Pearse, W. D., C. C. Davis, D. W. Inouye, R. B. Primack, and T. J. Davies, 2017: A statistical  
503 estimator for determining the limits of contemporary and historic phenology. *Nature ecology &*  
504 *evolution*, **1 (12)**, 1876.
- 505 Poppick, A., E. J. Moyer, and M. L. Stein, 2017: Estimating trends in the global mean temperature  
506 record. *Advances in Statistical Climatology, Meteorology and Oceanography*, **3 (1)**, 33–53, doi:  
507 10.5194/ascmo-3-33-2017, URL <http://www.adv-stat-clim-meteorol-oceanogr.net/3/33/2017/>.
- 508 Portnoy, S., and R. Koenker, 1997: The Gaussian hare and the laplacian tortoise: computability of  
509 squared-error versus absolute-error estimators. *Statistical Science*, **12 (4)**, 279–300.

510 Räisänen, J., 2002: CO<sub>2</sub>-induced changes in interannual temperature and precipitation variability  
 511 in 19 CMIP2 experiments. *Journal of Climate*, **15** (17), 2395–2411.

512 Reich, B. J., M. Fuentes, and D. B. Dunson, 2011: Bayesian spatial quantile regression. *Journal*  
 513 *of the American Statistical Association*, **106** (493), 6–20.

514 Rhines, A., K. A. McKinnon, M. P. Tingley, and P. Huybers, 2017: Seasonally resolved distribu-  
 515 tional trends of North American temperatures show contraction of winter variability. *Journal of*  
 516 *Climate*, **30** (3), 1139–1157.

517 Rodgers, K. B., J. Lin, and T. L. Frölicher, 2015: Emergence of multiple ocean ecosystem drivers  
 518 in a large ensemble suite with an Earth System Model. *Biogeosciences*, **12** (11), 3301.

519 Schneider, T., T. Bischoff, and H. Płotka, 2015: Physics of changes in synoptic midlatitude tem-  
 520 perature variability. *Journal of Climate*, **28** (6), 2312–2331.

521 Screen, J. A., 2014: Arctic amplification decreases temperature variance in northern mid-to high-  
 522 latitudes. *Nature Climate Change*, **4** (7), 577–582.

523 Semenov, V., and L. Bengtsson, 2002: Secular trends in daily precipitation characteristics: green-  
 524 house gas simulation with a coupled AOGCM. *Climate Dynamics*, **19** (2), 123–140.

525 Shields, C. A., D. A. Bailey, G. Danabasoglu, M. Jochum, J. T. Kiehl, S. Levis, and S. Park, 2012:  
 526 The low-resolution CCSM4. *Journal of Climate*, **25** (12), 3993–4014.

527 Singh, D., and Coauthors, 2014: Severe precipitation in Northern India in june 2013: causes,  
 528 historical context, and changes in probability. *Bulletin of the American Meteorological Society*,  
 529 **95** (9), S58.

530 Smith, R., and Coauthors, 2010: The parallel ocean program (POP) reference manual ocean com-  
 531 ponent of the Community Climate system Model (ccsm) and Community Earth System Model  
 532 (CESM). *Rep. LAUR-01853*, **141**.

533 Sriver, R. L., C. E. Forest, and K. Keller, 2015: Effects of initial conditions uncertainty on regional  
 534 climate variability: An analysis using a low-resolution CESM ensemble. *Geophysical Research*  
 535 *Letters*, **42 (13)**, 5468–5476.

536 Stainforth, D. A., S. C. Chapman, and N. W. Watkins, 2013: Mapping climate change in european  
 537 temperature distributions. *Environmental Research Letters*, **8 (3)**, 034 031.

538 Stott, P. A., D. A. Stone, and M. R. Allen, 2004: Human contribution to the European heatwave  
 539 of 2003. *Nature*, **432 (7017)**, 610–614.

540 Swain, D. L., M. Tsiang, M. Haugen, D. Singh, A. Charland, B. Rajaratnam, and N. S. Diffen-  
 541 baugh, 2014: The extraordinary California drought of 2013/2014: Character, context, and the  
 542 role of climate change. *Bulletin of the American Meteorological Society*, **95 (9)**, S3.

543 Thompson, D. W. J., E. A. Barnes, C. Deser, W. E. Foust, and A. S. Phillips, 2015: Quantifying  
 544 the role of internal climate variability in future climate trends. *Journal of Climate*, **28 (16)**,  
 545 6443–6456.

546 Trenberth, K. E., 2011: Attribution of climate variations and trends to human influences and  
 547 natural variability. *Wiley Interdisciplinary Reviews: Climate Change*, **2 (6)**, 925–930.

548 Trenberth, K. E., J. T. Fasullo, and T. G. Shepherd, 2015: Attribution of climate extreme events.  
 549 *Nature Climate Change*, **5 (8)**, 725–730.

550 **LIST OF TABLES**

551 **Table 1.** Degrees of freedom in the spline basis for each independent variable, with the  
552 interaction terms including the reduced set of seasonal polynomials with de-  
553 grees of freedom listed in the middle column. The temporal polynomials are  
554 the same in both the main and interaction terms. . . . . 30

	Seasonal	Seasonal-Int.	Temporal
1	5	3	3
2	7	3	3
3	10	3	3
4	10	3	4
5	12	3	4
6	15	3	4
7	15	3	5
8	15	5	5
9	18	5	5

TABLE 1. Degrees of freedom in the spline basis for each independent variable, with the interaction terms including the reduced set of seasonal polynomials with degrees of freedom listed in the middle column. The temporal polynomials are the same in both the main and interaction terms.

## LIST OF FIGURES

- Fig. 1.** An illustration of concepts and values related to distributions used in this paper. The cartoon shows a positively skewed (or “right-skewed”) probability distribution and the three quantile differences discussed in this paper, in the low tail, high tail, and middle of the distribution. The  $q$  quantile in a distribution is the value such that the probability of being below it has probability  $q$ . Here  $\Delta q_{\text{low}}$  is the difference between the 0.025 and 0.05 quantiles; the IQR or Interquartile Range that between the 0.25 and 0.75 quantiles; and  $\Delta q_{\text{high}}$  that between the 0.95 and 0.975 quantiles. The values  $\Delta q_{\text{low}}$  and  $\Delta q_{\text{high}}$  quantify variability in extreme values while IQR quantifies variability in the bulk of the distribution. . . . . 33
- Fig. 2.** Comparison of daily temperature distribution properties (mean, standard deviation, and skewness) between the CESM ensemble and ERA-Interim, for winter (DJF; aggregating all daily temperatures without deseasonalizing). We compare the years 1979-1994, the first available 15 years of the ERA-Interim dataset, and upscale the reanalysis from  $0.75^\circ$  to  $3.75^\circ$  resolution to match CESM. Units on top two rows are degrees Celsius; bottom row showing skewness is dimensionless. Winter skewness over the continental U.S. is negative in both model and reanalysis, implying a thicker lower tail; see Figure 1 and Appendix A1 for example and definitions. Overall, large-scale geospatial patterns are similar in both data sets, though some discrepancies are present (e.g. abnormally cold model Arctic winters). Letters **a-c** mark locations that will be used in examples throughout the paper; these are ordered from north to south, with latitudes and longitudes **a** ( $50.1, -101$ ), **b** ( $42.7, -82$ ), **c** ( $35.3, -98$ ). . . . . 34
- Fig. 3.** Illustration of results of our quantile estimation procedure using the 50-member CESM ensemble. The figure shows ensemble daily mean temperatures for the year 1850 for the three representative locations **a**, **b**, and **c** defined in Figure 2. The ensemble provides 50 points per day but for clarity we show only 10% of the data. Solid lines show the median daily temperature and dashed lines the .025 and .975 quantiles estimated by our procedure. (Note the higher variabilities in winter.) Note that the location of the points exceeding the smooth median estimate are approximately uniform across time (notwithstanding the amplitudes of residuals), suggesting that the quantile estimate is accurate for each day. XX put in Michael’s text here At all sites, the estimated quantile curves capture the seasonally changing patterns in the distributions reasonably well. . . . . 35
- Fig. 4.** Evolving distributions of daily mean temperature in the CESM ensemble RCP8.5 model runs at the locations **a**, **b**, **c** defined in Figure 2. Each distribution includes temperatures from a 15-day period over 15 model years for a total of 11,250 observations ( $15 \text{ days} \times 15 \text{ years} \times 50 \text{ ensemble members}$ ). Winter distributions are taken from Jan 1-15 and summer July 5-19; “initial” distributions include years 1850-1864 and “final” years 2096-2100. Changes in distributions are readily apparent, especially in winter at higher latitudes (locations **a** and **b**), but detailed quantification, especially of tail changes, requires more sophisticated techniques. . . . . 36
- Fig. 5.** Initial temperature distribution properties (left) and their changes over time (right) in the CESM ensemble RCP8.5 model runs, for aggregate wintertime (DJF) daily temperature. Initial (“pre-industrial”) and final periods are defined as in Figure 4, as 15-year periods 1850–1864 and 2086–2100. Distributional moments (mean, standard deviation, and skewness) are defined as in Figure 2. Units on the top two rows are degrees Celsius, while the bottom row showing skewness is dimensionless. Gray crosses mark locations where the changes are not significant at the 0.05 level, obtained by resampling the set of 50 simulations (with replacement) and recalculating the sample moments. *Top right:* Mean temperature universally increases. Extreme warming in the Hudson’s Bay region occurs where the model is biased low in present-day simulations. *Middle right:* As expected, standard deviation decreases strongly at higher latitudes. *Bottom right:* Changes in winter skewness show a dipole pattern, which enhances negative skew above  $\sim 40^\circ$  but reduces it at lower latitudes. . . . . 37
- Fig. 6.** As in Figure 5 but for aggregate summer (JJA) temperatures, and note that scales differ from those in Figure 5. Except in the desert Southwest and Mexico, changes in standard deviation (*middle right*) and skewness (*bottom right*) are generally smaller in summer than in winter and often not significant at the 0.05 level. . . . . 38

606	<b>Fig. 7.</b>	First day above freezing (solid lines) and $-2.2^{\circ}\text{C}$ (dashed lines) for each year from 1850-2100 as measured by fitting quantiles to average daily temperature of the CESM ensemble data set. Three quantiles are shown to capture the spread of the distribution, .5 (green), .25 (red) and .05 (black).	39
609	<b>Fig. 8.</b>	Changes in daily temperature variability (quantile differences) over time in CESM ensemble RCP8.5 runs estimated using our statistical approach. Because our approach removes the need to aggregate over time when presenting changes, we show here differences in distributions for a single day and year: Jan 1 for winter ( <i>top</i> ) and July 5 for summer ( <i>bottom</i> ), with differences evaluated between the years 1850 and 2100. Changes are expressed as fractions of initial variability, so that the value 0 indicates no change with respect to the initial year. <i>Left, middle, and right</i> columns show, respectively, changes in low tail variability, IQR, and high tail variability, as previously defined. Gray crosses mark grid points where the change is less than 3 standard deviations from the original estimate. As expected, estimated changes in IQR ( <i>middle</i> ) are similar to changes in standard deviation seen in Figures 5 and 6. Changes in tail variability are clearly different from those in IQR, meaning that future distributions are not simply a rescaling of the present-day distributions.	40
620	<b>Fig. 9.</b>	Evolving daily temperature variability (quantile differences) over time in CESM ensemble RCP8.5 runs estimated using our statistical approach, for locations <b>a</b> , <b>b</b> , and <b>c</b> . Using the analysis described in Figure 8, we show absolute IQR and tail variability as a function of seasonality, with different years (at 40 year intervals) shown as different colored lines, from 1850 (dark blue) to 2090 (dark red). Dashed lines represent pointwise 90% confidence intervals. Note the complexity of seasonal cycles in variability at different locations. These results show that the dipole pattern of changes in wintertime skewness changes seen in Figure 5 is driven by low rather than high tail behavior. In wintertime, in the more northern locations <b>a</b> and <b>b</b> , IQR reduces more strongly than does low tail variability, making skew more negative. In the more southern location <b>c</b> , IQR change is negligible while low tail variability reduces strongly, making skew more positive. In all locations, absolute changes in wintertime low tail variability are larger than changes in high tails. For fractional changes, see Supplementary Online Material Figure S6.	41
631	<b>Fig. 10.</b>	Exceedence probability of temperature events above the .95 quantile estimate. The density is obtained by making 10-day bins and counting the number of observations that are above the quantile estimate and normalizing by the total number of exceedences aggregated across all model runs. Each bin is represented by the bin start day, i.e. an x-axis value of 0 includes the interval $(0, 10]$ . We hold out 10 different sets of simulations to obtain 10 different estimates for each block of time, from which we calculate their mean shown as points and standard deviation shown as error bars around $\hat{\delta}_{test}$ .	42
637	<b>Fig. 11.</b>	Training and test exceedence standard deviation as a function of model number, where increasing model number signifies increasing degrees of freedom in the spline basis functions. The data were extracted from the gridbox located at $(\text{lat}, \text{lon}) = (31.5, -93.8)$ . The exceedence is calculated by binning seasonality in 10-day blocks and summing over the long term change.	43



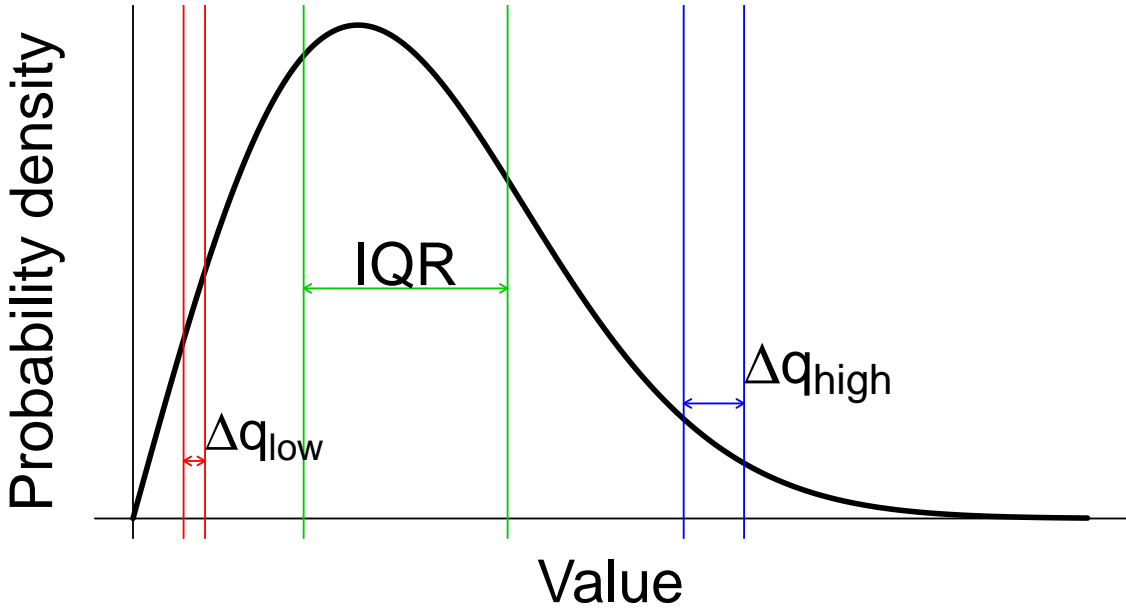


FIG. 1. An illustration of concepts and values related to distributions used in this paper. The cartoon shows a positively skewed (or “right-skewed”) probability distribution and the three quantile differences discussed in this paper, in the low tail, high tail, and middle of the distribution. The  $q$  quantile in a distribution is the value such that the probability of being below it has probability  $q$ . Here  $\Delta q_{\text{low}}$  is the difference between the 0.025 and 0.05 quantiles; the IQR or Interquartile Range that between the 0.25 and 0.75 quantiles; and  $\Delta q_{\text{high}}$  that between the 0.95 and 0.975 quantiles. The values  $\Delta q_{\text{low}}$  and  $\Delta q_{\text{high}}$  quantify variability in extreme values while IQR quantifies variability in the bulk of the distribution.

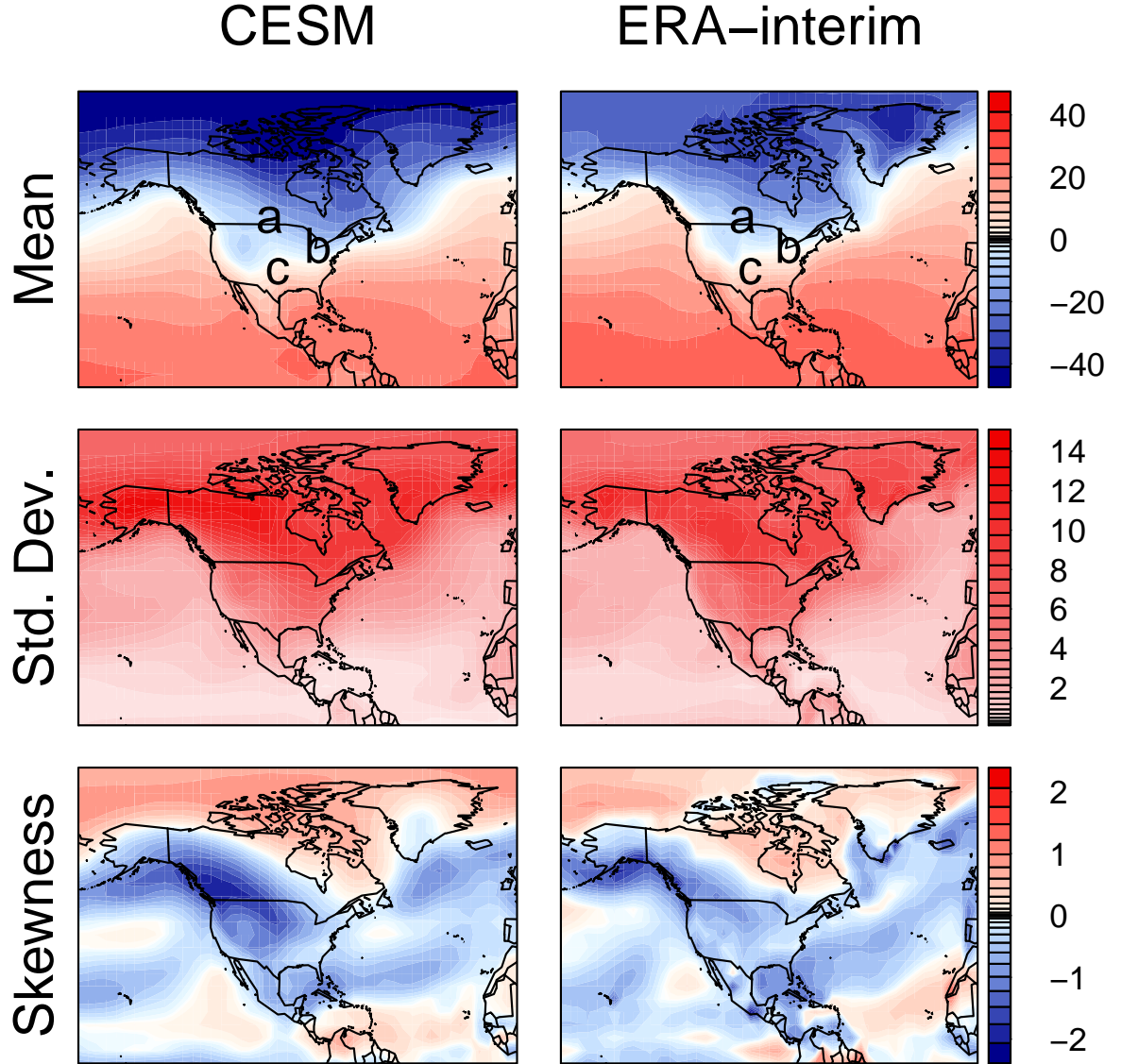
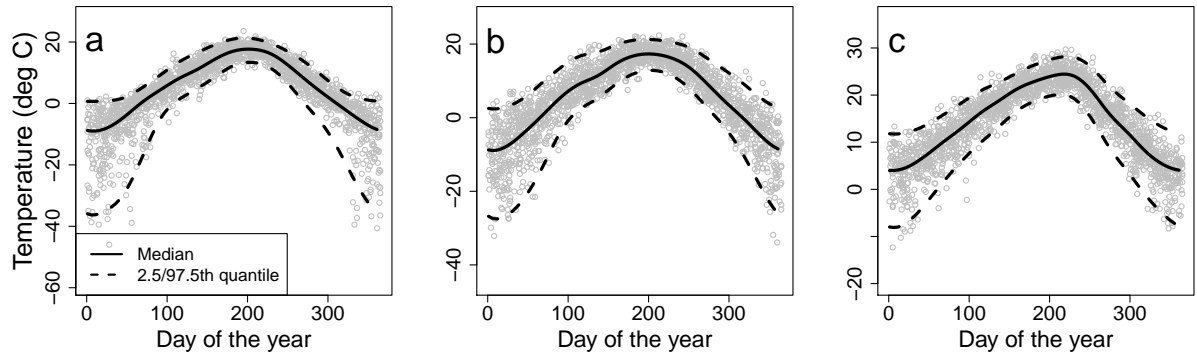


FIG. 2. Comparison of daily temperature distribution properties (mean, standard deviation, and skewness) between the CESM ensemble and ERA-Interim, for winter (DJF; aggregating all daily temperatures without deseasonalizing). We compare the years 1979-1994, the first available 15 years of the ERA-Interim dataset, and upscale the reanalysis from  $0.75^\circ$  to  $3.75^\circ$  resolution to match CESM. Units on top two rows are degrees Celsius; bottom row showing skewness is dimensionless. Winter skewness over the continental U.S. is negative in both model and reanalysis, implying a thicker lower tail; see Figure 1 and Appendix A1 for example and definitions. Overall, large-scale geospatial patterns are similar in both data sets, though some discrepancies are present (e.g. abnormally cold model Arctic winters). Letters **a-c** mark locations that will be used in examples throughout the paper; these are ordered from north to south, with latitudes and longitudes **a** ( $50.1, -101$ ), **b** ( $42.7, -82$ ), **c** ( $35.3, -98$ ).



655 FIG. 3. Illustration of results of our quantile estimation procedure using the 50-member CESM ensemble. The figure shows  
 656 ensemble daily mean temperatures for the year 1850 for the three representative locations **a**, **b**, and **c** defined in Figure 2. The  
 657 ensemble provides 50 points per day but for clarity we show only 10% of the data. Solid lines show the median daily temperature  
 658 and dashed lines the .025 and .975 quantiles estimated by our procedure. (Note the higher variabilities in winter.) Note that  
 659 the location of the points exceeding the smooth median estimate are approximately uniform across time (notwithstanding the  
 660 amplitudes of residuals), suggesting that the quantile estimate is accurate for each day. XX put in Michael's text here At all sites,  
 661 the estimated quantile curves capture the seasonally changing patterns in the distributions reasonably well.

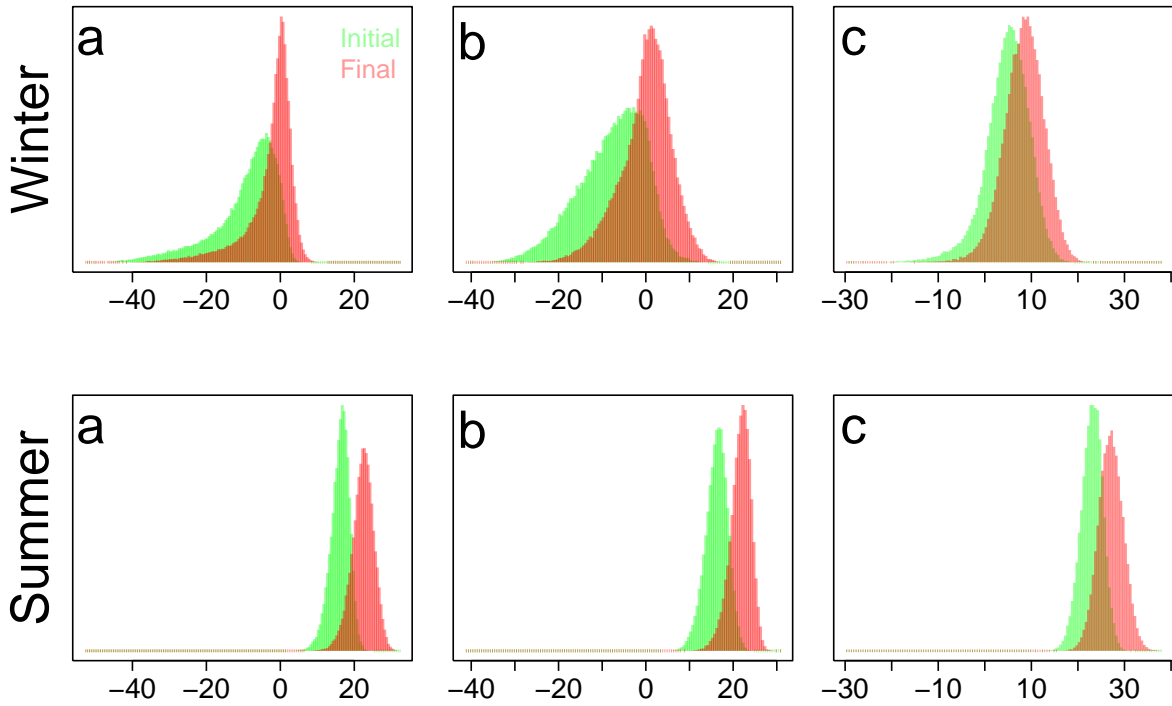


FIG. 4. Evolving distributions of daily mean temperature in the CESM ensemble RCP8.5 model runs at the locations **a**, **b**, **c** defined in Figure 2. Each distribution includes temperatures from a 15-day period over 15 model years for a total of 11,250 observations (15 days  $\times$  15 years  $\times$  50 ensemble members). Winter distributions are taken from Jan 1-15 and summer July 5-19; “initial” distributions include years 1850-1864 and “final” years 2096-2100. Changes in distributions are readily apparent, especially in winter at higher latitudes (locations **a** and **b**), but detailed quantification, especially of tail changes, requires more sophisticated techniques.

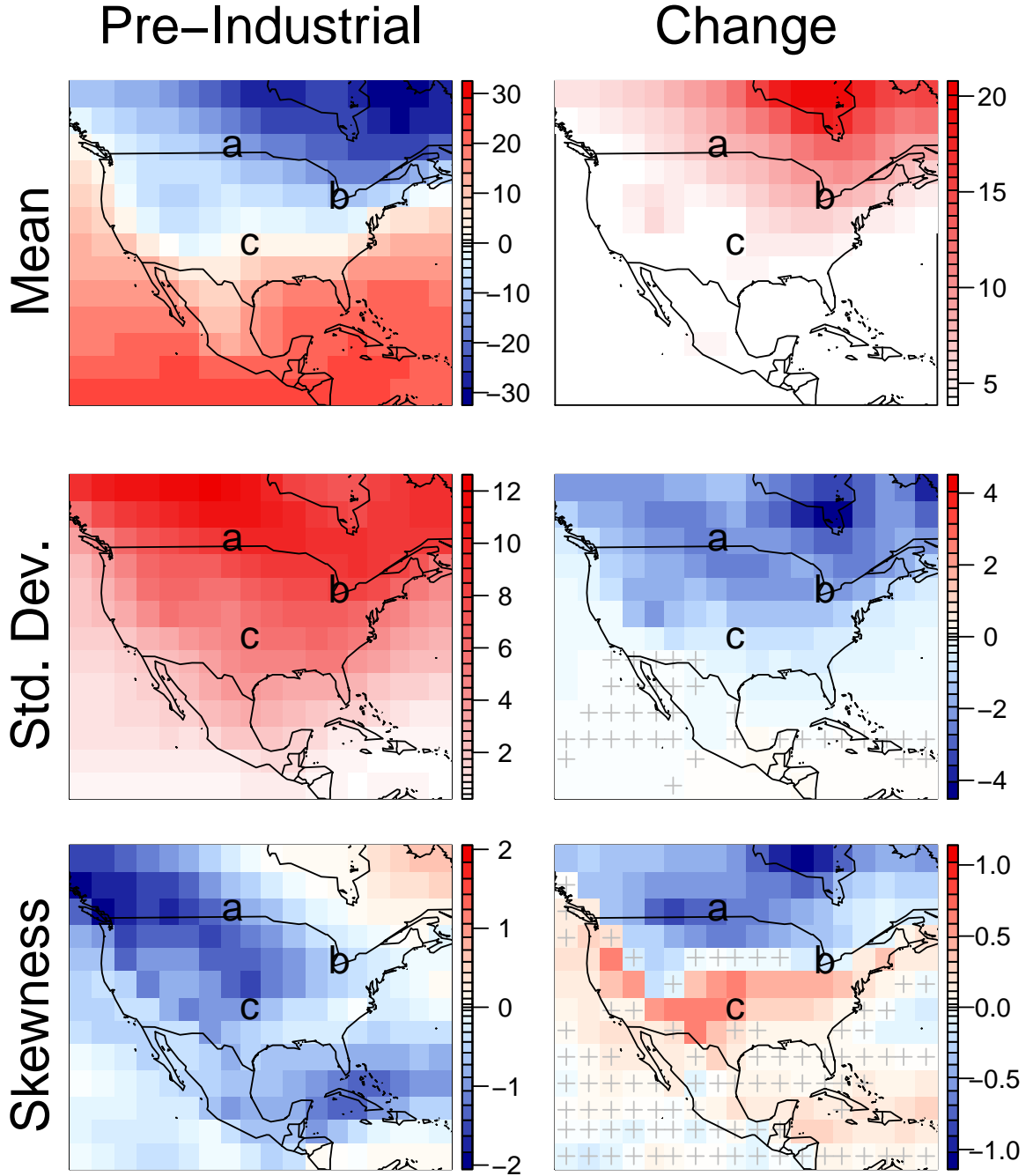


FIG. 5. Initial temperature distribution properties (left) and their changes over time (right) in the CESM ensemble RCP8.5 model runs, for aggregate wintertime (DJF) daily temperature. Initial (“pre-industrial”) and final periods are defined as in Figure 4, as 15-year periods 1850–1864 and 2086–2100. Distributional moments (mean, standard deviation, and skewness) are defined as in Figure 2. Units on the top two rows are degrees Celsius, while the bottom row showing skewness is dimensionless. Gray crosses mark locations where the changes are not significant at the 0.05 level, obtained by resampling the set of 50 simulations (with replacement) and recalculating the sample moments. *Top right:* Mean temperature universally increases. Extreme warming in the Hudson’s Bay region occurs where the model is biased low in present-day simulations. *Middle right:* As expected, standard deviation decreases strongly at higher latitudes. *Bottom right:* Changes in winter skewness show a dipole pattern, which enhances negative skew above  $\sim 40^\circ$  but reduces it at lower latitudes.

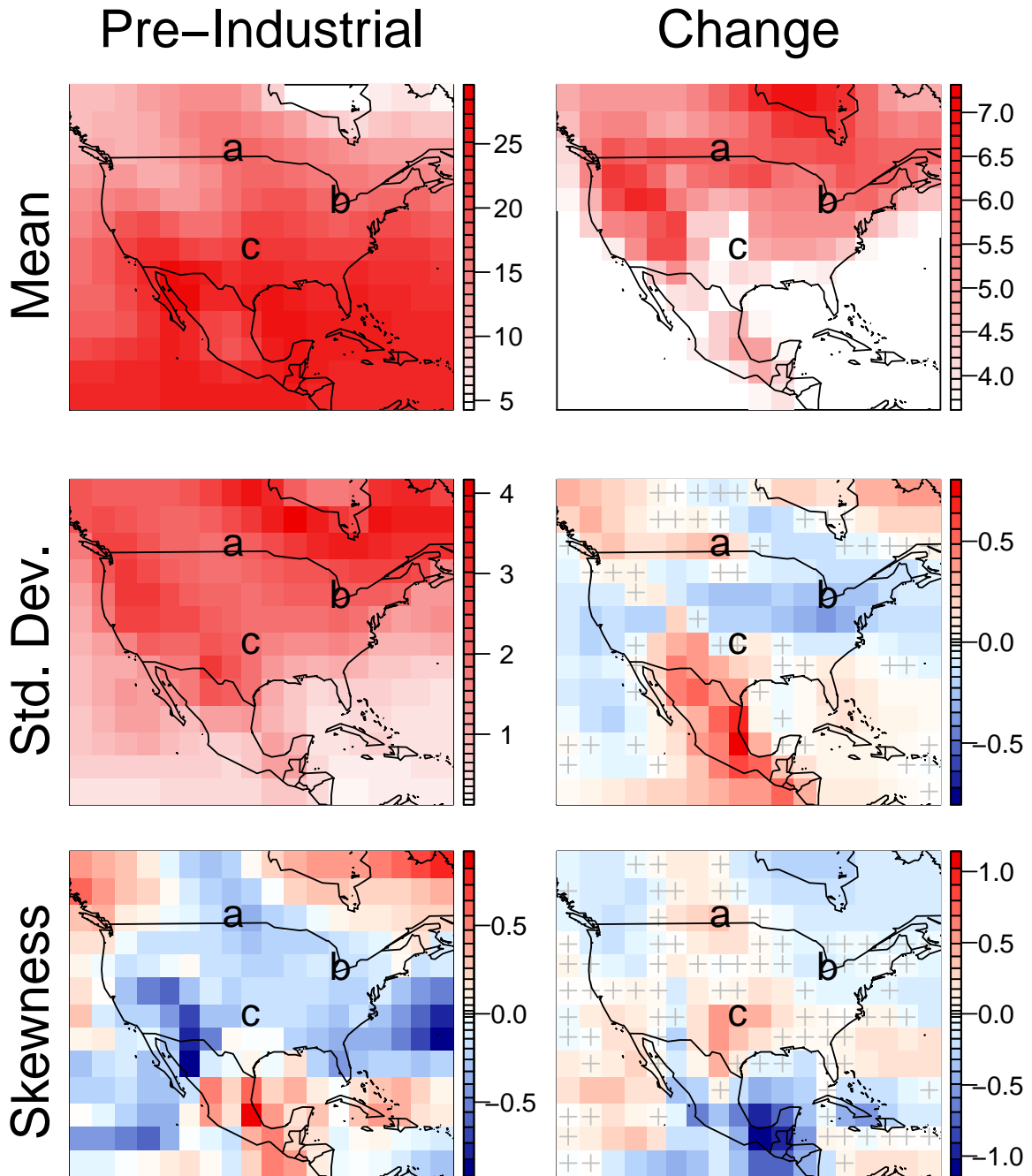


FIG. 6. As in Figure 5 but for aggregate summer (JJA) temperatures, and note that scales differ from those in Figure 5. Except in the desert Southwest and Mexico, changes in standard deviation (*middle right*) and skewness (*bottom right*) are generally smaller in summer than in winter and often not significant at the 0.05 level.

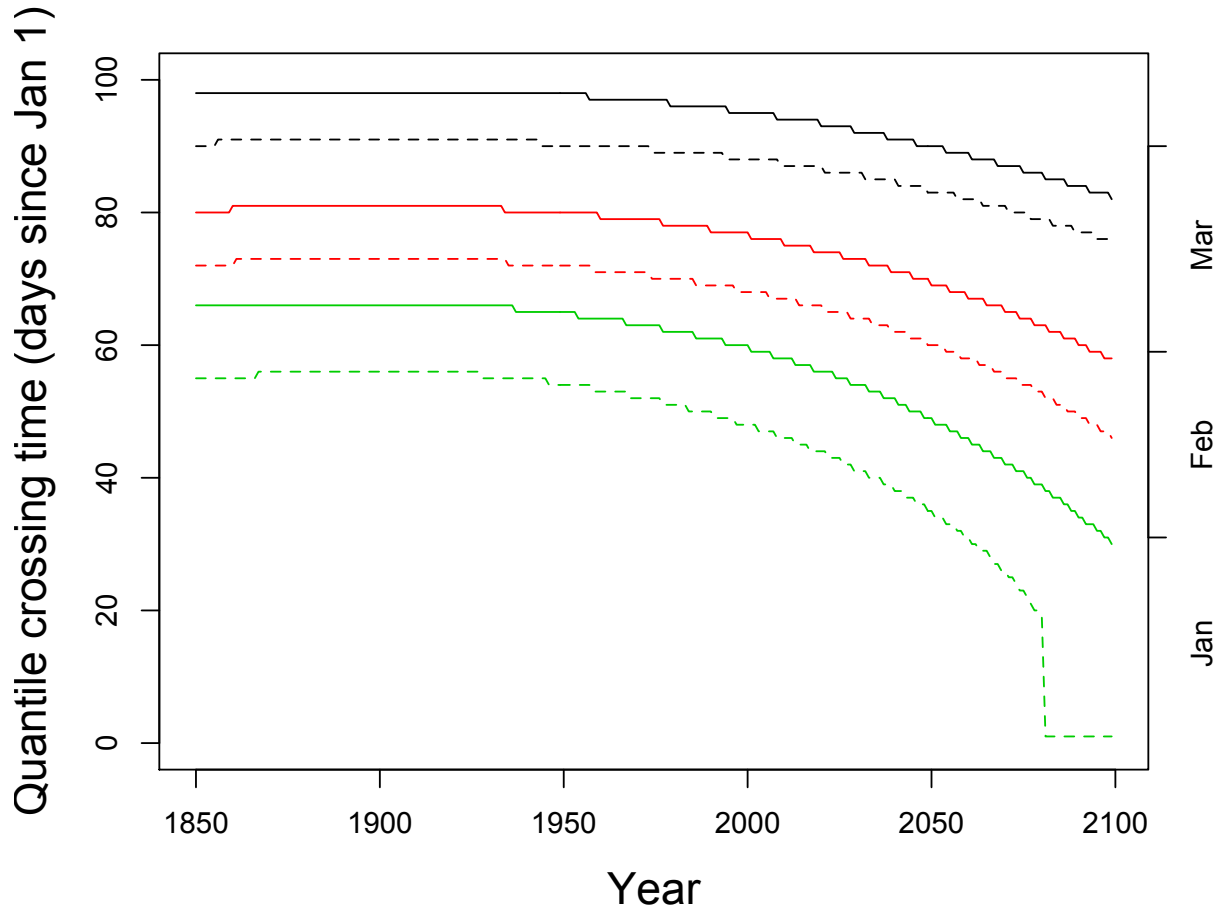
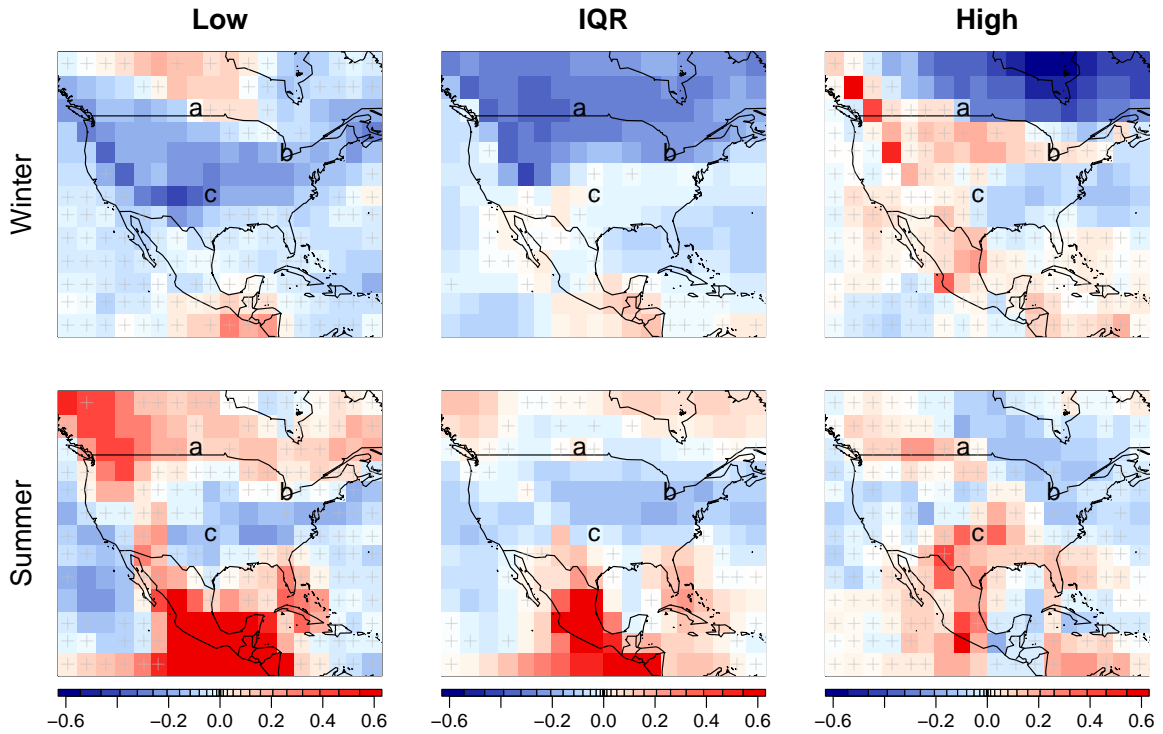


FIG. 7. First day above freezing (solid lines) and  $-2.2^{\circ}\text{C}$  (dashed lines) for each year from 1850-2100 as measured by fitting quantiles to average daily temperature of the CESM ensemble data set. Three quantiles are shown to capture the spread of the distribution, .5 (green), .25 (red) and .05 (black).



683 FIG. 8. Changes in daily temperature variability (quantile differences) over time in CESM ensemble RCP8.5 runs estimated  
 684 using our statistical approach. Because our approach removes the need to aggregate over time when presenting changes, we show  
 685 here differences in distributions for a single day and year: Jan 1 for winter (*top*) and July 5 for summer (*bottom*), with differences  
 686 evaluated between the years 1850 and 2100. Changes are expressed as fractions of initial variability, so that the value 0 indicates  
 687 no change with respect to the initial year. *Left*, *middle*, and *right* columns show, respectively, changes in low tail variability, IQR,  
 688 and high tail variability, as previously defined. Gray crosses mark grid points where the change is less than 3 standard deviations  
 689 from the original estimate. As expected, estimated changes in IQR (*middle*) are similar to changes in standard deviation seen in  
 690 Figures 5 and 6. Changes in tail variability are clearly different from those in IQR, meaning that future distributions are not simply  
 691 a rescaling of the present-day distributions.



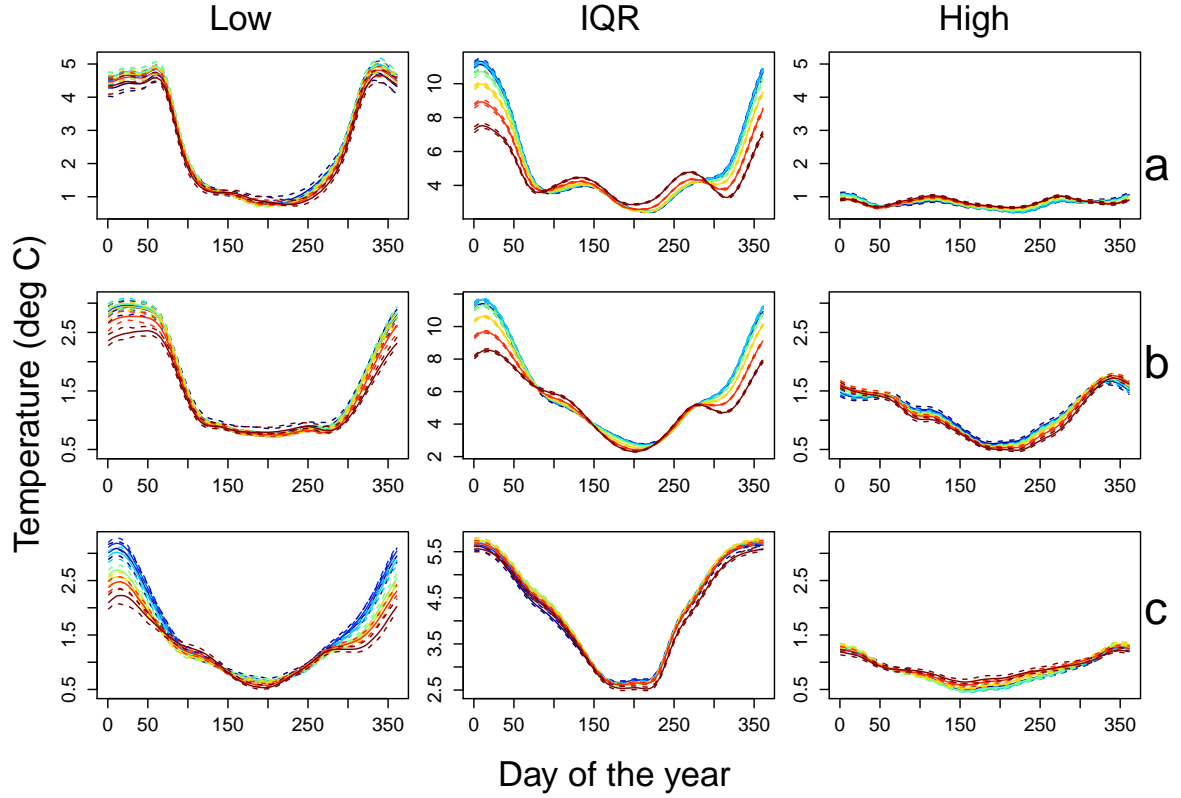
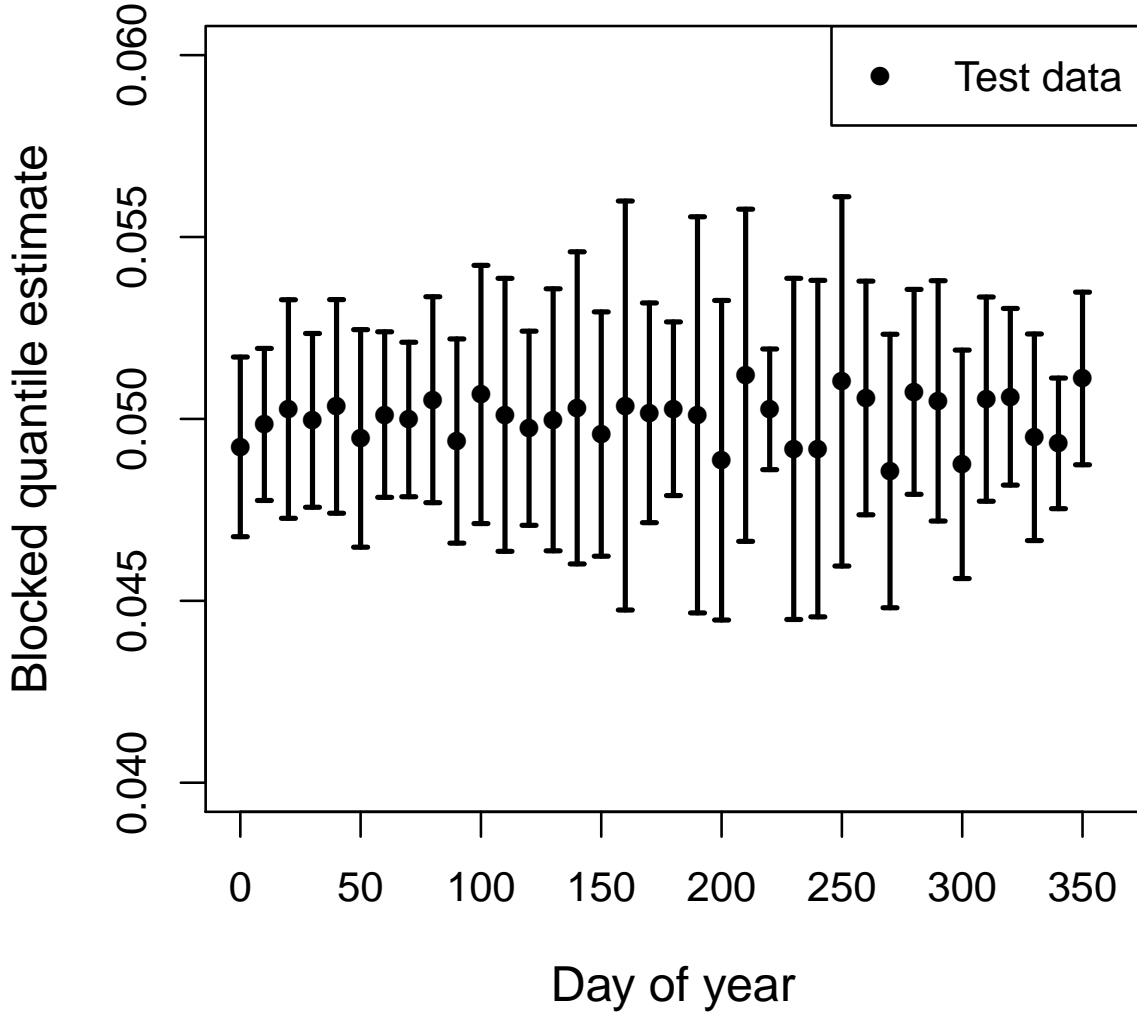


FIG. 9. Evolving daily temperature variability (quantile differences) over time in CESM ensemble RCP8.5 runs estimated using our statistical approach, for locations **a**, **b**, and **c**. Using the analysis described in Figure 8, we show absolute IQR and tail variability as a function of seasonality, with different years (at 40 year intervals) shown as different colored lines, from 1850 (dark blue) to 2090 (dark red). Dashed lines represent pointwise 90% confidence intervals. Note the complexity of seasonal cycles in variability at different locations. These results show that the dipole pattern of changes in wintertime skewness changes seen in Figure 5 is driven by low rather than high tail behavior. In wintertime, in the more northern locations **a** and **b**, IQR reduces more strongly than does low tail variability, making skew more negative. In the more southern location **c**, IQR change is negligible while low tail variability reduces strongly, making skew more positive. In all locations, absolute changes in wintertime low tail variability are larger than changes in high tails. For fractional changes, see Supplementary Online Material Figure S6.



701 FIG. 10. Exceedence probability of temperature events above the .95 quantile estimate. The density is obtained by making  
 702 10-day bins and counting the number of observations that are above the quantile estimate and normalizing by the total number of  
 703 exceedences aggregated across all model runs. Each bin is represented by the bin start day, i.e. an x-axis value of 0 includes the  
 704 interval  $(0, 10]$ . We hold out 10 different sets of simulations to obtain 10 different estimates for each block of time, from which we  
 705 calculate their mean shown as points and standard deviation shown as error bars around  $\hat{S}_{test}$ .

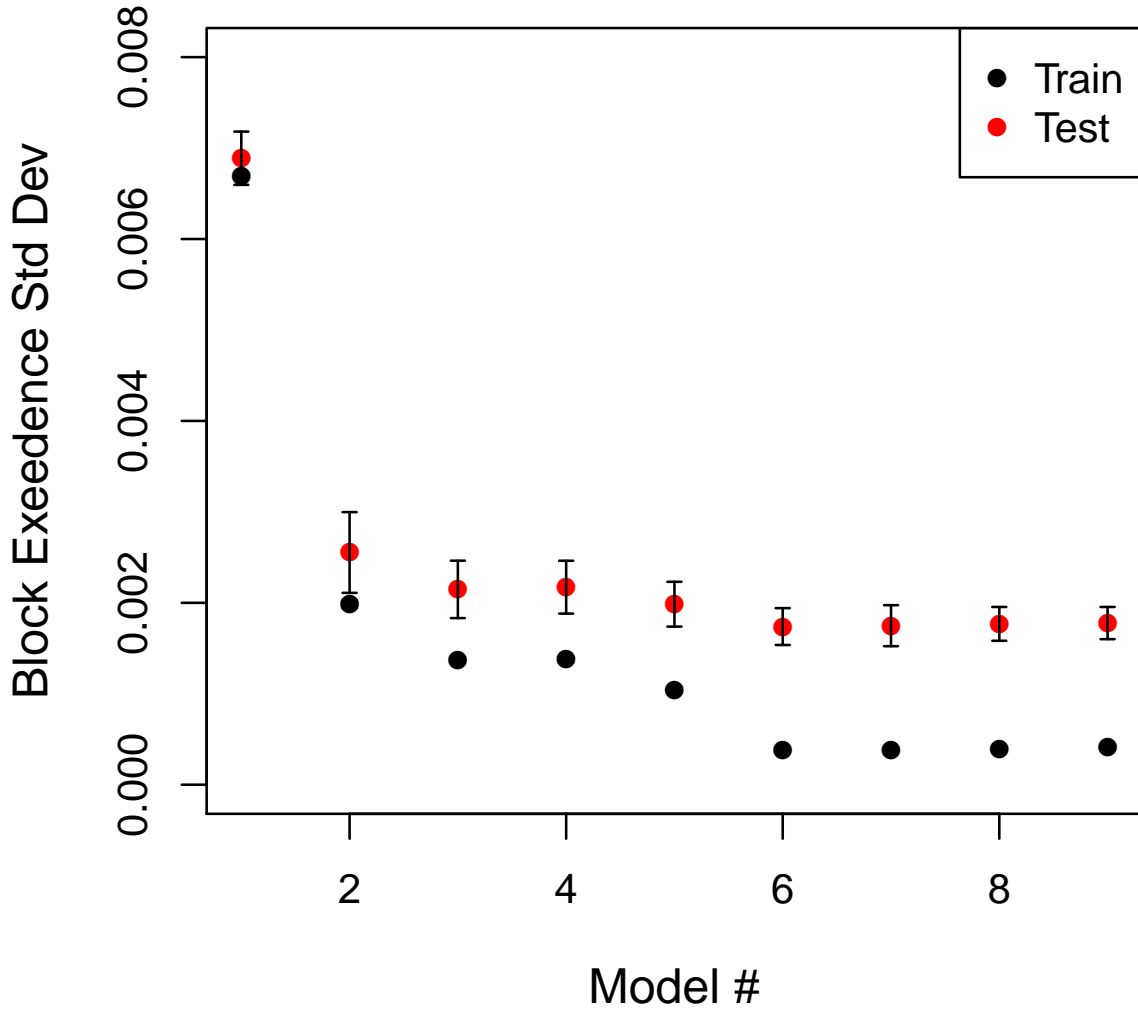


FIG. 11. Training and test exceedence standard deviation as a function of model number, where increasing model number signifies increasing degrees of freedom in the spline basis functions. The data were extracted from the gridbox located at (lat, lon) = (31.5, -93.8). The exceedence is calculated by binning seasonality in 10-day blocks and summing over the long term change.